Transactions Letters

A Comparative Study of Iterative Channel Estimators for Mobile OFDM Systems

Frieder Sanzi, Sven Jelting, and Joachim Speidel, *Member, IEEE*

***Abstract*—In this letter, we investigate two iterative channel estimators for mobile orthogonal-frequency division multiplexing. The first estimator is based on iterative filtering and decoding whereas the second one uses an *a posteriori* probability (APP) algorithm. The first method consists of two cascaded one-dimensional Wiener filters, which interpolate the unknown time-varying two-dimensional frequency response in between the known pilot symbols. As will be shown, the performance can be increased by feeding back the likelihood values at the output of the APP-decoder to iteratively compute an improved estimate of the channel frequency response. The second method applies two APP estimators, one for the frequency and the other one for the time direction. The two estimators are embedded in an iterative loop similar to the turbo decoding principle. As will be shown in detail, this iterative estimator is superior and its performance is independent of whether the chosen time-frequency pilot grid satisfies the two-dimensional sampling theorem or not. The bit-error rate as a function of the signal-to-noise ratio is used as a performance measure. In addition, the convergence of the iterative decoding loop is studied with the extrinsic information transfer chart.**

***Index Terms*—Channel estimation (CE), iterative decoding, orrhogonal-frequency division multiplexing (OFDM).**

I. Introduction

THE TIME-VARYING propagation conditions of the mobile communication channel make channel estimation (CE) for multicarrier systems a demanding task at the receiver. To allow for coherent detection, the two-dimensional channel transfer function must be estimated. To support estimation, often pilot symbols are periodically inserted into the transmitted signal. Typically, the CE is performed by cascading two one-dimensional finite-impulse response (FIR) interpolation filters whose coefficients are based on the minimum mean square error (MMSE) criterion, as described, e.g., in [1].

In [2], the authors propose a technique for CE with iterative filtering and decoding in a flat-fading environment for a single-carrier binary phase-shift keying modulation scheme. The idea is to feed back information from the output of the channel decoder to the estimation stage. The estimator can improve its performance, because it gets not only the information from the pilots, but also reliability information of the coded bits. So, the CE can now be performed by a one-dimensional FIR interpolation filter which operates at a higher sampling rate. A further reduction of the bit-error rate (BER) is achieved by iterative estimation and decoding. In this letter, we extend this idea of iterative filtering and decoding to a multicarrier scenario with quaternary phase-shift keying (QPSK) modulation.

Another method to estimate and track the channel in a multicarrier system is based on the calculation of the *a posteriori* probability [(APP) CE], as described in [3] and [4]. The estimation of the two-dimensional channel transfer function is performed by a concatenation of two one-dimensional APP estimators in time and frequency direction, respectively. As will be shown, this method also enables iterative estimation and decoding at the receiver to further reduce the BER.

In this letter, the performance of the different iterative channel estimators is evaluated on the basis of BER charts. In addition, the convergence of the iterative decoding loop is studied with the extrinsic information transfer chart (EXIT chart), recently introduced in [5]–[7].

This letter is organized as follows. In Section II, the system model of the transmitter and the mobile channel is presented. In Section III, the two different iterative CE methods are described in detail: CE with iterative filtering and decoding and the iterative APP CE. The comparison of the performance of the channel estimators for different mobile channels by computer simulation is presented in Section IV. The BER as a function of the signal-to-noise ratio E_b/N_0 is used as a performance measure. Also in this section, the convergence behavior of the iterative decoding loop is studied with the EXIT chart. Finally, Section V concludes the letter.

II. System Model

A. Transmitter

The block diagram of the transmitter is given in Fig. 1. The sequence b_ν from the binary source is encoded by a convolutional encoder. Its output signal c_μ consists of the coded bits. The next block is the interleaver, which outputs the signal $\tilde{c}_\mu$. After interleaving, two successive coded bits $\tilde{c}_{2\cdot\xi}$ and $\tilde{c}_{2\cdot\xi+1}$ are grouped and mapped onto a QPSK symbol Z_ξ with alphabet $\pm 1 \pm j$ according to

$$Z_\xi = f_{\mathrm{map},2}(\tilde{c}_{2\cdot\xi}, \tilde{c}_{2\cdot\xi+1}). \tag{1}$$

A separate binary source generates the pilot bits a_ε. In order to obtain the pilot symbols, two successive pilot bits

Manuscript received August 13, 2001; revised March 27, 2002 and November 27, 2002; accepted December 11, 2002. The editor coordinating the review of this paper and approving it for publication is C. Tellambura.

F. Sanzi and J. Speidel are with the Institute of Telecommunications, University of Stuttgart, 70569 Stuttgart, Germany (e-mail: sanzi@inue.uni-stuttgart.de; speidel@inue.uni-stuttgart.de).

S. Jelting is with the Institute for Systems Theory and Display Technology, University of Stuttgart, 70569 Stuttgart, Germany (e-mail: sven.jelting@lfb.unistuttgart.de).

Digital Object Identifier 10.1109/TWC.2003.817436

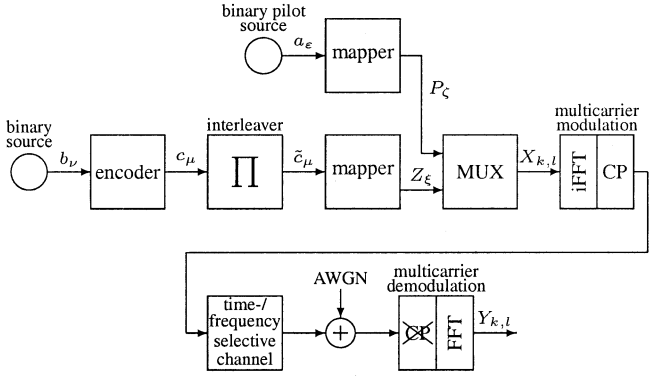

Fig. 1. Transmitter and channel model.

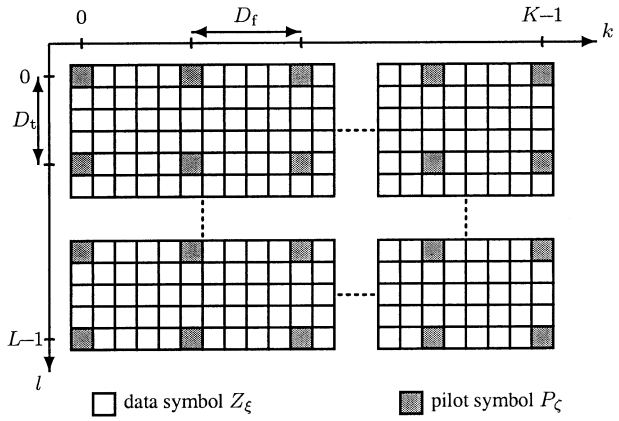

Fig. 2. Multiplexing scheme for signal $X_{k,l}$.

$a_{2\cdot\zeta}$ and $a_{2\cdot\zeta+1}$ are grouped and mapped onto a QPSK symbol P_ζ. The mapping rule for the pilot bits a_ε is the same as for the coded bits $\tilde{c}_\mu$.

After the mappings, the symbols Z_ξ and P_ζ are multiplexed in order to form the signal $X_{k,l}$. The multiplexing scheme is shown in Fig. 2.

After multiplexing, the signal $X_{k,l}$ is modulated onto K orthogonal subcarriers by an inverse fast Fourier transform (iFFT)-block (see Fig. 1). The transmission is done on a block-by-block basis, with blocks of K subcarriers in frequency and L orthogonal-frequency division multiplexing (OFDM) symbols in time direction. As shown in Fig. 2, the distance of the pilot symbols in frequency direction is D_f and in time direction D_t. After iFFT, the guard interval or cyclic prefix (CP) is inserted. The output signal of the multicarrier modulation is fed into the channel.

B. Channel Model

For the mobile channel, we use the wide-sense stationary uncorrelated scattering (WSSUS) channel model introduced in [8]. The time-varying frequency response of the channel can be expressed as

$$H(f,t)=\frac{1}{\sqrt{M}}\sum_{i=1}^{M}e^{j(\varphi_i+2\pi f_{D_i}t-2\pi f\tau_i)} \tag{2}$$

where f and t are continuous frequency and time, respectively, φ_i is the phase, f_{D_i} the Doppler frequency, and τ_i the delay of the ith path. M denotes the number of propagation paths. The φ_i, f_{D_i}, and τ_i are randomly chosen depending on the corresponding joint probability density function (pdf) $p_{\varphi,f_D,\tau}(\varphi,f_D,\tau)$ of the considered channel model. We assume φ,τ, and f_D to be mutually independent [8]. Hence, the joint pdf can be expressed as

$$p_{\varphi,f_D,\tau}(\varphi,f_D,\tau)=p_\varphi(\varphi)\cdot p_{f_D}(f_D)\cdot p_\tau(\tau). \tag{3}$$

We use a channel model where the phase φ is uniformly distributed between 0 and 2π. For the delay τ, we assume an exponential pdf

$$p_\tau(\tau)=\begin{cases}\frac{e^{-\tau/\tau_{\rm rms}}}{\tau_{\rm rms}(1-e^{-\tau_{\max}/\tau_{\rm rms}})}, & 0\le\tau\le\tau_{\max}\\ 0, & \text{otherwise}\end{cases} \tag{4}$$

whereby, $\tau_{\max}$ is the channel delay spread. $\tau_{\rm rms}$ is chosen such that $p_\tau(\tau_{\max})/p_\tau(0)=1/1000$. The pdf of the Doppler frequency is assumed to be of Jakes' type

$$p_{f_D}(f_D)=\begin{cases}\frac{1}{\pi f_{D_{\max}}\sqrt{1-(f_D/f_{D_{\max}})^2}}, & |f_D|<f_{D_{\max}}\\ 0, & \text{otherwise}\end{cases} \tag{5}$$

whereby, $f_{D_{\max}}$ is the maximal Doppler shift.

With these assumptions, the complex autocorrelation function of $H(f,t)$ in frequency direction is given by [9]

$$R_{f;k}=\frac{1-e^{-\tau_{\max}\left(\frac{1}{\tau_{\rm rms}}+j2\pi\cdot k\cdot\Delta f\right)}}{\left(1-e^{-\frac{\tau_{\max}}{\tau_{\rm rms}}}\right)\cdot(1+j2\pi\cdot k\cdot\Delta f\cdot\tau_{\rm rms})} \tag{6}$$

whereby, Δf is the subcarrier spacing and k is the discrete frequency index. For the autocorrelation function of $H(f,t)$ with respect to t, we obtain [9]

$$R_{t;l}=J_0\left(2\pi f_{D_{\max}}\cdot l\cdot T_s\right) \tag{7}$$

whereby, T_s is the duration of one OFDM symbol (useful part plus guard interval), l is the discrete time index, and J_0 is the Bessel function of zero order.

As a consequence of (3), we can compute the expected value

$$E\left\{H_{k,l}\cdot H^*_{k',l'}\right\}=R_{f;(k-k')}\cdot R_{t;(l-l')} \tag{8}$$

whereby, $*$ denotes the conjugate complex operation.

C. Receiver

In the following, we assume that the channel characteristic in (2) is approximately unchanged during the duration T_s of one OFDM symbol. Under this assumption and provided that the guard interval is longer than the delay spread of the channel, the CP avoids intercarrier interference as well as intersymbol interference. In this case, we obtain the received QPSK constellation points $Y_{k,l}$ in Fig. 1 after removal of the CP and multicarrier demodulation with FFT

$$Y_{k,l}=H_{k,l}\cdot X_{k,l}+N_{k,l} \tag{9}$$

whereby, l is the OFDM symbol index, k is the subcarrier index, $X_{k,l}$ are the transmitted signal constellation points, and $N_{k,l}$ are statistically independent and identically distributed complex Gaussian noise variables with component-wise noise

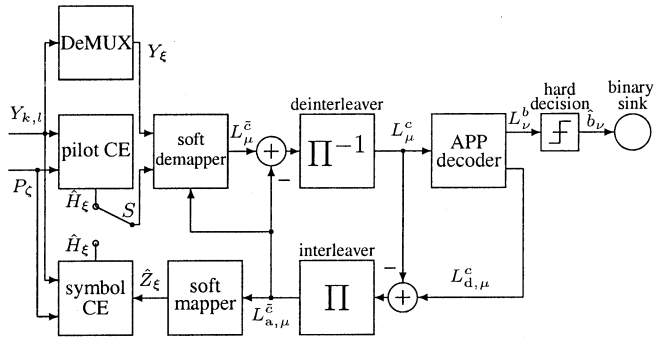

Fig. 3. Receiver for CE with iterative filtering and decoding.

power $\sigma_N^2 = N_0/2$. The $H_{k,l}$ are sample values of the channel frequency response

$$H_{k,l} = H(k \cdot \Delta f, l \cdot T_s). \tag{10}$$

The two iterative channel estimators, which we compare in this letter, will be described in Section III.

III. Iterative Channel Estimation

A. CE With Iterative Filtering and Decoding

For this case, the receiver is given in Fig. 3. The first block is the pilot-based CE (pilot CE). At this stage, the channel frequency response is known at the pilot positions with

$$\tilde{H}_{k,l} = \frac{Y_{k,l}}{X_{k,l}} = H_{k,l} + \tilde{N}_{k,l} \quad \text{and} \quad \tilde{N}_{k,l} = \frac{N_{k,l}}{X_{k,l}}. \tag{11}$$

In (11), k and l denote a pilot position. Therefore, k and l fulfill the conditions

$$k \operatorname{Mod} D_f = 0 \quad \text{and} \quad l \operatorname{Mod} D_t = 0 \tag{12}$$

whereby, Mod is the modulo operator. The expected value $E\{\tilde{N}_{k,l} \cdot \tilde{N}^*_{k',l'}\}$ with $\tilde{N}_{k,l}$ in (11) can be expressed as [9]

$$E\left\{\tilde{N}_{k,l} \cdot \tilde{N}^*_{k',l'}\right\} = N_0 \cdot \beta \cdot \delta_{k-k',l-l'} \quad \text{and}$$
$$\beta = E\left\{\frac{1}{|X_{k,l}|^2}\right\}. \tag{13}$$

To allow for coherent detection, the receiver has to know the channel frequency response over the whole time-frequency grid. Therefore, the remaining $H_{k,l}$ have to be interpolated based on the known $\tilde{H}_{k,l}$. The CE is typically performed by cascading two one-dimensional FIR filters, one for the frequency direction k and the other one for the time direction l [1], [10], [11].

We start with filtering in frequency direction. The order of filtering (time or frequency first) for a rectangular pilot grid, as shown in Fig. 2, is arbitrary due to the linearity of the scheme. So, the filtering in frequency direction for OFDM symbol l_0 with $l_0 \operatorname{Mod} D_t = 0$ is given by

$$\tilde{H}'_{k,l_0} = \sum_{m=1}^{P} w_m^{k,l_0} \cdot \tilde{H}_{k_m,l_0} \tag{14}$$

whereby, $\{k_m, l_0\}$ are the P nearest pilot positions to the actual position $\{k, l_0\}$ with $k_m \operatorname{Mod} D_f = 0$. For the filter coefficients w_m^{k,l_0} in (14), which minimize $E\{|H_{k,l_0} - \tilde{H}'_{k,l_0}|^2\}$ (Wiener filter), we can derive [12]

$$\mathbf{w}_k^T = \mathbf{r}^T_{H\tilde{H},k} \cdot \mathbf{R}^{-1}_{\tilde{H}\tilde{H}} \tag{15}$$

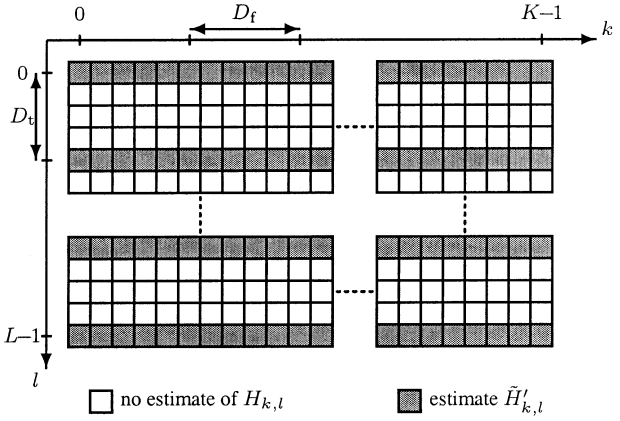

Fig. 4. Positions of estimates $\tilde{H}'_{k,l}$ of $H_{k,l}$.

with

$$\mathbf{w}_k^T = \left(w_1^{k,l_0}, \ldots, w_P^{k,l_0}\right) \tag{16}$$

$$\mathbf{r}^T_{H\tilde{H},k} = \left(R_{f;(k-k_1)}, \ldots, R_{f;(k-k_P)}\right) \tag{17}$$

and

$$\mathbf{R}_{\tilde{H}\tilde{H}} = \begin{pmatrix} R_{f;(k_1-k_1)} + N_0 \cdot \beta & \cdots & R_{f;(k_1-k_P)} \\ \vdots & \ddots & \vdots \\ R_{f;(k_P-k_1)} & \cdots & R_{f;(k_P-k_P)} + N_0 \cdot \beta \end{pmatrix}. \tag{18}$$

The MMSE $E\{|H_{k,l_0} - \tilde{H}'_{k,l_0}|^2\}$ can be calculated as follows [12]:

$$E\left\{\left|H_{k,l_0} - \tilde{H}'_{k,l_0}\right|^2\right\} = J^k_{\min} = 1 - \mathbf{r}^T_{H\tilde{H},k} \cdot \mathbf{R}^{-1}_{\tilde{H}\tilde{H}} \cdot \mathbf{r}^*_{H\tilde{H},k}. \tag{19}$$

After this filtering in frequency direction, estimates $\tilde{H}'_{k,l}$ of $H_{k,l}$ are available for every OFDM symbol l with $l \operatorname{Mod} D_t = 0$. Fig. 4 illustrates this aspect in the k, l plane.

After this operation, the filtering in the time direction l follows. Similar to (14), the filtering in time direction l for subcarrier k_0 with $0 \le k_0 \le K-1$ can be expressed as

$$\hat{H}_{k_0,l} = \sum_{m=1}^{Q} v_m^{k_0,l} \cdot \tilde{H}'_{k_0,l_m} \tag{20}$$

whereby, $\{k_0, l_m\}$ are the Q nearest positions to the actual position $\{k_0, l\}$ with $l_m \operatorname{Mod} D_t = 0$ of the known estimates $\tilde{H}'_{k_0,l_m}$.

Similar to (15), the optimal filter coefficients can be computed as

$$\mathbf{v}_l^T = \mathbf{r}^T_{H\tilde{H}',l} \cdot \mathbf{R}^{-1}_{\tilde{H}'\tilde{H}'} \tag{21}$$

with

$$\mathbf{v}_l^T = \left(v_1^{k_0,l}, \ldots, v_Q^{k_0,l}\right) \tag{22}$$

$$\mathbf{r}^T_{H\tilde{H}',l} = \left(1 - J^{k_0}_{\min}\right) \cdot \left(R_{t;(l-l_1)}, \ldots, R_{t;(l-l_Q)}\right) \tag{23}$$

and

$$\mathbf{R}_{\tilde{H}'\tilde{H}'} = \begin{pmatrix} 1 - J^{k_0}_{\min} & \cdots & R_{t;(l_1-l_Q)} \cdot J_{\mathbf{w}} \\ \vdots & \ddots & \vdots \\ R_{t;(l_Q-l_1)} \cdot J_{\mathbf{w}} & \cdots & 1 - J^{k_0}_{\min} \end{pmatrix} \tag{24}$$

with

$$J_{\mathbf{w}} = 1 - J_{\min}^{k_0} - N_0 \cdot \beta \cdot \left(\mathbf{w}_{k_0}^T \cdot \mathbf{w}_{k_0}^*\right). \quad (25)$$

For the determination of the vector $\mathbf{r}_{H\tilde{H}',l}$, the expected value $E\{\tilde{H}'_{k_0,l_m} \cdot (\tilde{H}'_{k_0,l_{\tilde{m}}})^*\}$ is required [12]. It can be computed as

$$E\left\{H_{k_0,l}\left(\tilde{H}'_{k_0,l_m}\right)^*\right\} \overset{(14)}{=} E\left\{H_{k_0,l}\sum_{n=1}^{P}\left(w_n^{k_0,l_m}\cdot\tilde{H}_{k_n,l_m}\right)^*\right\}. \quad (26)$$

Owing to the rectangular pilot grid in Fig. 2, the filter coefficients $w_n^{k_0,l_m}$ fulfill the following condition:

$$w_n^{k_0,l_m} = w_n^{k_0,l_0}. \quad (27)$$

Using (27), the expected value in (26) becomes

$$\begin{aligned} E\left\{H_{k_0,l}\left(\tilde{H}'_{k_0,l_m}\right)^*\right\} &\overset{(27)}{=} \sum_{n=1}^{P}\left(w_n^{k_0,l_0}\right)^* E\left\{H_{k_0,l}\cdot\tilde{H}^*_{k_n,l_m}\right\} \\ &\overset{(8)}{=} R_{t;(l-l_m)}\sum_{n=1}^{P}\left(w_n^{k_0,l_0}\right)^*\cdot R_{f;(k_0-k_n)} \\ &\overset{(19)}{=} R_{t;(l-l_m)}\cdot\left(1-J_{\min}^{k_0}\right). \end{aligned} \quad (28)$$

To find the matrix $\mathbf{R}_{\tilde{H}'\tilde{H}'}$, we need the expected value $E\{\tilde{H}'_{k_0,l_m} \cdot (\tilde{H}'_{k_0,l_{\tilde{m}}})^*\}$ [12]. Using (14), we obtain

$$\begin{aligned} &E\left\{\tilde{H}'_{k_0,l_m}\cdot\left(\tilde{H}'_{k_0,l_{\tilde{m}}}\right)^*\right\} \\ &= E\left\{\sum_{n=1}^{P} w_n^{k_0,l_m}\cdot\tilde{H}_{k_n,l_m}\cdot\sum_{i=1}^{P}\left(w_i^{k_0,l_{\tilde{m}}}\cdot\tilde{H}_{k_i,l_{\tilde{m}}}\right)^*\right\}. \end{aligned} \quad (29)$$

Taking (8), (15), (16), (18), (27), and (28) into account, the expected value in (29) becomes

$$\begin{aligned} E\left\{\tilde{H}'_{k_0,l_m}\cdot\left(\tilde{H}'_{k_0,l_{\tilde{m}}}\right)^*\right\} =& R_{t;(l_m-l_{\tilde{m}})}\cdot\left(1-J_{\min}^{k_0}\right) \\ &+ N_0\beta\left(\mathbf{w}_{k_0}^T\cdot\mathbf{w}_{k_0}^*\right) \\ &\cdot\left(\delta_{l_m-l_{\tilde{m}}} - R_{t;(l_m-l_{\tilde{m}})}\right) \end{aligned} \quad (30)$$

After filtering in time direction l for all subcarriers, we have found the estimates $\hat{H}_{k,l}$ of $H_{k,l}$ over the whole k,l plane. The resulting MMSE is given by [12]

$$E\{|H_{k,l} - \tilde{H}_{k,l}|^2\} = J_{\min}^{k,l} = 1 - \mathbf{r}_{H\tilde{H}',l}^T \cdot \mathbf{R}_{\tilde{H}'\tilde{H}'}^{-1} \cdot \mathbf{r}_{H\tilde{H}',l}^*. \quad (31)$$

After pilot CE in Fig. 3, the demapper follows. The input signals to the demapper are Y_ξ and $\hat{H}_\xi$ (switch S in upper position). Note, that Y_ξ are the received constellations points after demultiplexing. The demultiplexer (DeMUX) block discards parts of the received signal, in which pilot symbols are present. $\hat{H}_\xi$ are the estimates of H_ξ at the positions where data symbols are transmitted. Now, the demapper needs to calculate log-likelihood ratios $L_\mu^{\tilde{c}}$ (L-values [13]) of two coded bits $\tilde{c}_\mu$ and $\tilde{c}_{\mu+1}$ with $\mu\text{Mod}2 = 0$ for each incoming QPSK symbol $Y_{\mu\text{Div}2}$, where Div is the integer division operator. The L-value of bit $\tilde{c}_\mu$ conditioned on $Y_{\mu\text{Div}2}$ can be calculated as follows [14]:

$$L_\mu^{\tilde{c}} = L(\tilde{c}_\mu \,|\, Y_{\mu\text{Div}2}) = L_{a,\mu}^{\tilde{c}} + \ln\frac{A_{10} + A_{11}\cdot e^{L_{a,\mu+1}^{\tilde{c}}}}{A_{00} + A_{01}\cdot e^{L_{a,\mu+1}^{\tilde{c}}}} \quad (32)$$

with

$$A_{ij} = p_N(Y_{\mu\text{Div}2} \,|\, \tilde{c}_\mu = i, \tilde{c}_{\mu+1} = j) \quad (33)$$

and

$$L_{a,\mu}^{\tilde{c}} = \ln\frac{\Pr[\tilde{c}_\mu = 1]}{\Pr[\tilde{c}_\mu = 0]}. \quad (34)$$

If H_ξ is available (perfect CE) at the receiver, then the pdf p_N can be expressed as [14]

$$p_N(Y_\eta \,|\, \tilde{c}_\mu, \tilde{c}_{\mu+1}) = \frac{1}{2\pi\sigma_N^2} e^{-\frac{1}{2\sigma_N^2}|Y_\eta - H_\eta\cdot f_{\text{map},2}(\tilde{c}_\mu,\tilde{c}_{\mu+1})|^2} \quad (35)$$

whereby, $\eta = \mu\text{Div}2$. Otherwise, p_N can be calculated as in [15]

$$P_N(Y_\eta \,|\, \tilde{c}_\mu, \tilde{c}_{\mu+1}) = \frac{1}{2\pi\sigma_\eta^2} e^{-\frac{1}{2\sigma_\eta^2}|Y_n - \tilde{H}_\eta\cdot f_{\text{map},2}(\tilde{c}_\mu,\tilde{c}_{\mu+1})|^2} \quad (36)$$

$2\sigma_\eta^2$ in (36) is given by [15]

$$2\sigma_\eta^2 = 2\sigma_N^2 + J_{\min}^{\eta(k,l)}\cdot E_S \quad (37)$$

whereby, $J_{\min}^{\eta(k,l)} = E\{|H_\eta - \hat{H}_\eta|^2\}$ according to (31) and $E_S = E\{|X_\eta|^2\}$.

After bitwise deinterleaving in Fig. 3 and soft-in/soft-out decoding with an APP algorithm [13], [16], the L-values L_ν^b of the transmitted information bits are available at the output of the APP decoder. Hard decision yields the estimates $\hat{b}_\nu$ of the transmitted information bits, which are fed into the binary sink.

To allow for iterative decoding, the extrinsic information $L_{d,\mu}^c - L_\mu^c$ of the coded bits in Fig. 3 is fed back [2]. After interleaving, the extrinsic information becomes *a priori* knowledge $L_{a,\mu}^{\tilde{c}}$, which is fed into the soft demapper and into the soft mapper.

The soft mapper calculates the symbols $\hat{Z}_\xi$ as follows:

$$\hat{Z}_\xi = B_{00} + B_{01} + B_{10} + B_{11} \quad (38)$$

with

$$\begin{aligned} B_{ij} = \Pr[\tilde{c}_{2\xi} = i]\cdot\Pr[\tilde{c}_{2\xi+1} = j] \\ \cdot f_{\text{map},2}(\tilde{c}_{2\cdot\xi} = i, \tilde{c}_{2\cdot\xi+1} = j) \end{aligned} \quad (39)$$

Using (34), the probabilities $\Pr[\tilde{c}_{2\xi} = 1]$ and $\Pr[\tilde{c}_{2\xi} = 0]$ can be expressed as

$$\Pr[\tilde{c}_{2\xi} = 1] = \frac{1}{2}\left(1 + \tanh\left(\frac{L_{a,2\xi}^{\tilde{c}}}{2}\right)\right) \quad (40)$$

and

$$\Pr[\tilde{c}_{2\xi} = 0] = \frac{1}{2}\left(1 - \tanh\left(\frac{L_{a,2\xi}^{\tilde{c}}}{2}\right)\right). \quad (41)$$

The probabilities $\Pr[\tilde{c}_{2\xi+1}=1]$ and $\Pr[\tilde{c}_{2\xi+1}=0]$ are calculated similarly to (40) and (41). After the soft mapper, the symbol-based CE stage (symbol CE) in Fig. 3 follows. It computes the estimates $\tilde{H}_\zeta^P$ and $\tilde{H}_\xi$ with

$$\tilde{H}_\zeta^P = \frac{Y_\zeta^P}{P_\zeta} \quad \text{and} \quad \tilde{H}_\xi = \frac{Y_\xi}{\tilde{Z}_\xi} = \frac{Y_\xi}{|\tilde{Z}_\xi|^2}\cdot \hat{Z}_\xi^* \tag{42}$$

in a first step, whereby, Y_ζ^P are the received constellation points at the pilot positions. Due to the QPSK modulation, we know *a priori*, that $|Z_\xi|$ is independent of ξ. So, $|Z_\xi|^2 = |Z|^2 = 2$. Using this fact, we can refine (42) in the following way:

$$\tilde{H}_\xi = \frac{Y_\xi}{2}\cdot \hat{Z}_\xi^*. \tag{43}$$

$\tilde{H}_\zeta^P$ and $\tilde{H}_\xi$ are then multiplexed in order to form the signal $\tilde{H}_{k,l}$. With this procedure, estimates $\tilde{H}_{k,l}$ of $H_{k,l}$ over the whole k,l plane and not only at the pilot positions as in the pilot CE stage have been found.

According to the method in [2], another CE has to be performed as a second step at the symbol CE stage in Fig. 3. Similar to the pilot CE stage, this estimation is done by cascading two one-dimensional FIR filters, one for the frequency direction k and the other one for the time direction l. We start with the frequency direction k, and the filtering for OFDM symbol l_0 with $0 \le l_0 \le L-1$ can be calculated as

$$\tilde{H}_{k,l_0} = \sum_{\substack{\tilde{k}=k-\tilde{K}\\ \tilde{k}\neq k}}^{\tilde{k}=k+\tilde{K}} v_{\tilde{k}}^{k,l_0}\cdot \tilde{H}_{\tilde{k},l_0}. \tag{44}$$

The filter coefficients $v_{\tilde{k}}^{k,l_0}$ in (44) are also based on the MMSE criterion [12] according to (15) with the assumption that we have perfect *a priori* knowledge $L_{a,\mu}^{\tilde{c}}$ at the input of the soft mapper. From (44), we see that the estimated channel frequency response $\tilde{H}'_{k,l_0}$ is given by the interpolation using samples of the estimates $\tilde{H}_{\tilde{k},l_0}$ at $\tilde{K}$ subcarrier positions before and $\tilde{K}$ subcarriers after subcarrier k. The estimate $\tilde{H}_{k,l_0}$ from subcarrier k is not used as in [2]. We see from (44) that $\tilde{H}'_{k,l_0}$ is independent of the pilot symbol spacing.

Now, the filtering in time direction l follows. Therefore, we consider a subcarrier k_0 with $0 \le k_0 \le K-1$. Similar to (44), the filtering in time direction l for subcarrier k_0 can be expressed as

$$\hat{H}_{k_0,l} = \sum_{\substack{\tilde{l}=l-\tilde{L}\\ \tilde{l}\neq l}}^{\tilde{l}=l+\tilde{L}} v_{\tilde{l}}^{k_0,l}\cdot \tilde{H}'_{k_0,\tilde{l}}. \tag{45}$$

The filter coefficients $v_{\tilde{l}}^{k_0,l}$ in (45) are also based on the MMSE criterion [12] according to (21).

After finalizing this procedure for all subcarriers, we have found the estimates $\hat{H}_{k,l}$ of $H_{k,l}$ over the whole k,l plane. The resulting MMSE $E\{|H_{k,l}-\hat{H}_{k,l}|^2\}$ can be calculated in the same manner as in (31).

After this computation, the switch S in Fig. 3 is put into the lower position to close the iteration loop. The output $\hat{H}_\xi$ of the symbol CE stage is fed into the demapper and a second iteration pass can start, etc.

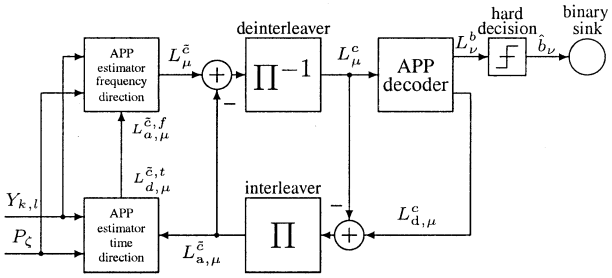

Fig. 5. Receiver with iterative APP CE.

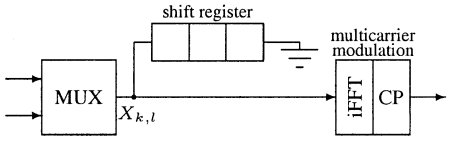

Fig. 6. Virtual shift register at the transmitter.

B. Iterative APP CE

The receiver with iterative APP CE is depicted in Fig. 5, [3], [4]. For APP estimation, the symbol-by-symbol maximum *a posteriori* (MAP)-algorithm, according to [16], is applied to an appropriately chosen metric. To help understanding, the symbols $X_{k,l}$ at the transmitter in Fig. 1 can be thought of being put into a virtual shift register at the output of the multiplexer (MUX). This is shown in Fig. 6. Owing to this "artificial grouping," the corresponding trellis [17] exploits the time and frequency continuity of the channel transfer function at the receiver.

At time index l, the logarithmic metric increment of the APP estimation in time direction, assuming QPSK-modulated signals, can be simplified for subcarrier k_0 with $0 \le k_0 \le K-1$ to [15]

$$\gamma_l = -\frac{\left|Y_{k_0,l}-\hat{H}_{k_0,l}^t\cdot \hat{X}_{k_0,l}\right|^2}{2\cdot\sigma_t^2} + \sum_{i=0}^{1} d_{k_0,l}^i\cdot L_{a,k_0,l}^{t,i} \tag{46}$$

with estimated channel coefficient (linear FIR prediction of order m_t)

$$\hat{H}_{k_0,l}^t = \sum_{i=1}^{m_t} u_{t,i}\cdot \frac{Y_{k_0,l-i}}{\hat{X}_{k_0,l-i}} \tag{47}$$

whereby, the FIR filter coefficients $u_{t,i}$ are calculated with the Wiener–Hopf equation based on the time autocorrelation $R_{t;1}$ of the channel frequency response [12], [15]. The $\hat{X}_{k_0,l} \in \{\pm 1 \pm j\}$ denote the hypothesized transmitted data or pilot symbols according to the trellis structure, and $L_{a,k_0,l}^{t,i}$ are the *a priori* L-values, which are formed by multiplexing the *a priori* L-values $L_{a,\mu}^{\tilde{c}}$ of the coded bits $\tilde{c}_\mu$ and the *a priori* L-values $L_{a,\varepsilon}^{a}$ of the pilot bits a_ε. According to (34), the L-values $L_{a,\varepsilon}^{a}$ can be expressed as

$$L_{a,\varepsilon}^{a} = \ln\frac{\Pr[a_\varepsilon=1]}{\Pr[a_\varepsilon=0]}. \tag{48}$$

The bits $d^0_{k_0,l}$ and $d^1_{k_0,l}$ in the sum in (46) result from the hard demapping of $\hat{X}_{k_0,l}$

$$\left(d^0_{k_0,l}, d^1_{k_0,l}\right) = f^{-1}_{\mathrm{map},2}\left(\hat{X}_{k_0,l}\right). \tag{49}$$

The term $2\sigma_t^2$ in (46) is the variance of the estimation error in time direction according to (37), [15].

Accordingly, at frequency index k, the APP estimation in frequency direction is characterized for OFDM symbol l_0 with $0 \le l_0 \le L-1$ by the metric increment

$$\gamma_k = -\frac{\left|Y_{k,l_0} - \hat{H}^f_{k,l_0} \cdot \hat{X}_{k,l_0}\right|^2}{2\cdot\sigma_f^2} + \sum_{i=0}^{1} d^i_{k,l_0} \cdot L^{f,i}_{a,k,l_0} \tag{50}$$

with estimated channel coefficient

$$\hat{H}^f_{k,l_0} = \sum_{i=1}^{m_f} u_{f,i} \cdot \frac{Y_{k-i,l_0}}{\hat{X}_{k-i,l_0}} \tag{51}$$

whereby, the FIR filter coefficients $u_{f,i}$ are based on the frequency autocorrelation function $R_{f;k}$, [12]. The $L^{f,i}_{a,k,l_0}$ denote the *a priori* L-values, which are formed by multiplexing the L-values $L^{\tilde{c},f}_{a,\mu}$ and the L-values $L^a_{a,\varepsilon}$. The term $2\sigma_f^2$ in (50) is the variance of the estimation error in frequency direction similar as in (46).

Separate one-dimensional APP estimation in time and frequency direction is possible owing to the two-dimensional continuity of the time-varying channel frequency response. The channel coefficient $H_{k,l}$ changes smoothly rather than abruptly in time and frequency direction.

The inputs to the APP estimator in time direction are the noise and fading affected channel observations $Y_{k,l}$, i.e., the unprocessed discrete time signal from the channel, the pilot symbols P_ζ, and the *a priori* L-values $L^{\tilde{c}}_{a,\mu}$. Note, that the APP estimator processes the *a priori* L-values $L^a_{a,\varepsilon}$ of the pilot bits. The L-values $L^a_{a,\varepsilon}$ are taken as "perfect *a priori* knowledge" by the APP estimation, i.e., as big L-values with positive or negative sign. For the remaining positions, the *a priori* L-values $L^{\tilde{c}}_{a,\mu}$ are set to zero for the very first pass through the estimator. The APP estimator in time direction outputs the estimated L-values $L^{\tilde{c},t}_{d,\mu}$, which are forwarded as *a priori* input $L^{\tilde{c},f}_{a,\mu} = L^{\tilde{c},t}_{d,\mu}$ to the APP estimator in frequency direction. This estimator uses the *a priori* input $L^{\tilde{c},f}_{a,\mu}$, the channel observations $Y_{k,l}$, and the *a priori* L-values $L^a_{a,\varepsilon}$ of the pilot bits to calculate improved L-values $L^{\tilde{c}}_{\mu}$. After subtracting *a priori* knowledge $L^{\tilde{c}}_{a,\mu}$ from the output, the difference signal is passed on to the deinterleaver for further processing in the APP decoder.

IV. Comparison of the Two-Iterative Channel Estimators by Simulation

We use the following channel and multicarrier system parameters: duration of one OFDM-symbol $T_s = 312.5$ μs and subcarrier spacing $\Delta f = 4$ kHz. Therefore, the duration of the guard interval is $T_g = 62.5$ μs. In principle, the guard interval (CP) adds redundancy. So, the rate R_g including the CP becomes

$$R_g = \frac{T_s - T_g}{T_s} = 0.8. \tag{52}$$

The pilot symbols are arranged in a rectangular grid, as shown in Fig. 2. The distance of the pilot symbols in frequency direction is $D_f = 10$ and in time direction $D_t = 10$. For the blockwise transmission, we use $K = 1001$ adjacent subcarriers and $L = 101$ consecutive OFDM symbols. Therefore, the pilot symbol rate R_P is

$$R_P = \frac{K\cdot L - (K \operatorname{Div} D_f + 1)\cdot(L \operatorname{Div} D_t + 1)}{K\cdot L} = 0.989\,011. \tag{53}$$

For the QPSK modulation, we use Gray mapping with two bits per symbol. With the above parameters, the interleaving depth V_L becomes

$$V_L = 2\cdot R_P \cdot K \cdot L = 199\,980. \tag{54}$$

As an example, the used convolutional code is recursive systematic with feedback polynomial $G_r = 037$ (octal notation), feedforward polynomial $G = 023$, Memory 4, and code rate $R_c = 0.5$. Note that in the following, all E_b/N_0-values are given with respect to the overall information rate

$$R = R_c \cdot R_P \cdot R_g = 0.395\,604\,4. \tag{55}$$

The following simulations are done for mobile channels ($M = 100$) with different maximal Doppler shifts $f_{D_{\max}}$ to see the influence of the fading rate on the performance of the estimators. As a performance measure, we take the BER at the output of the hard decision device of the receivers in Figs. 3 and 5. In addition to that, we apply the EXIT chart [5]–[7] to gain more insight into the convergence behavior of the iterative decoding loop. In all examples, the maximal channel delay spread is $\tau_{\max} = 20$ μs.

A. CE With Iterative Filtering and Decoding

For the pilot CE stage in Fig. 3, the $P = 6$ nearest pilot symbols are used for interpolation in frequency direction [see (14)]. For the interpolation in time direction, we use $Q = 6$ in (20). In order to get a good estimation result out of the pilot CE stage, the pilot grid has to fulfill the two-dimensional sampling theorem [1], [10], [11], [18]. Therefore, the "sampling frequency" $1/(D_t \cdot T_s)$ in time direction has to meet the condition $1/(D_t \cdot T_s) > 2 \cdot f_{D_{\max}}$. For the given $T_s = 312.5$ μs and $D_t = 10$, the maximal Doppler shift $f_{D_{\max}} < 160$ Hz results. The "sampling frequency" $1/(D_f \cdot \Delta f)$ in frequency direction has to fulfill $1/(D_f \cdot \Delta f) > \tau_{\max}$. For $\Delta f = 4$ kHz and $D_f = 10$, the maximal delay is restricted to $\tau_{\max} < 25$ μs. As we assume channels with $\tau_{\max} = 20$ μs in all our simulations, the two-dimensional sampling theorem is always fulfilled in the frequency direction.

For the symbol CE stage, we consider the case $\tilde{K} = 5$ and $\tilde{L} = 5$ in (44) and (45). We are interested in the influence of the maximal Doppler shift $f_{D_{\max}}$ on the performance of this receiver. Critical channels are those with maximal Doppler shift $f_{D_{\max}} > 160$ Hz.

Fig. 7 shows the mutual information transfer characteristics of the detection stage, consisting of the soft mapper, the symbol CE stage, and the demapper with the switch S in the lower position.

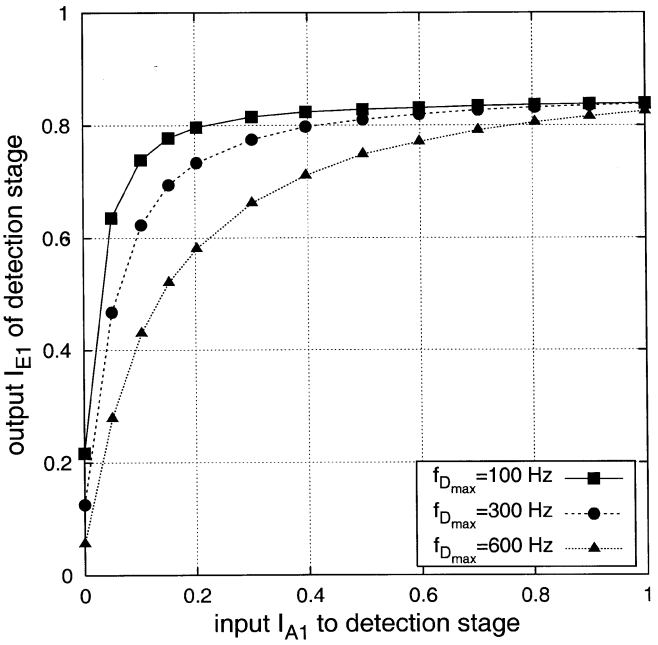

Fig. 7. Mutual information transfer characteristics of the detection stage consisting of the soft mapper, the symbol CE stage, and the demapper for different maximal Doppler shifts $f_{D\max}$ at $E_b/N_0 = 10$ dB.

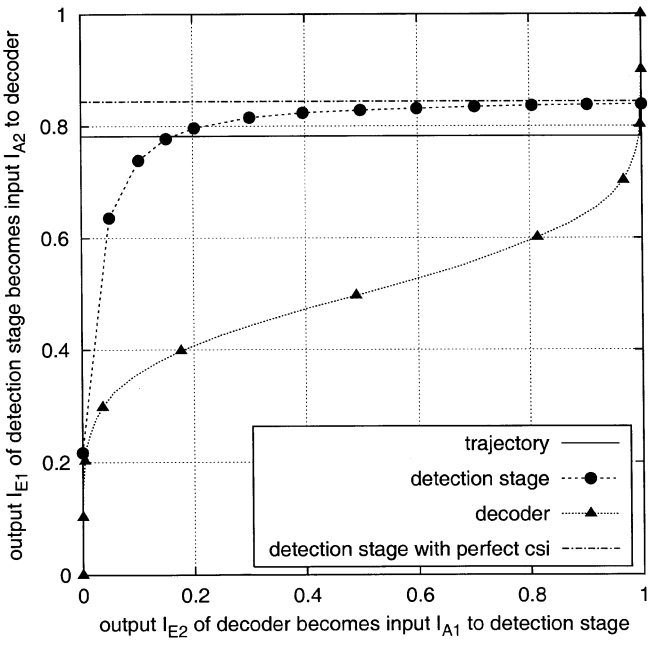

Fig. 8. EXIT chart, detection stage, and decoder with simulated trajectory of the iterative decoding loop for $f_{D\max} = 100$ Hz at $E_b/N_0 = 10$ dB.

The *a priori* input $L^{\tilde{c}}_{a,\mu}$ to the detection stage is on the abscissa (mutual information $0 \leq I_{A1} \leq 1$ in bit per binary symbol). The *a posteriori* output $L^{\tilde{c}}_{\mu} - L^{\tilde{c}}_{a,\mu}$ is on the ordinate (mutual information $0 \leq I_{E1} \leq 1$). The mutual information transfer characteristics describe the input–output relations of the detection stage and are calculated by applying a Gaussian distributed random variable as *a priori* input and quantifying the *a posteriori* output in terms of mutual information [3]–[7]. As can be seen, the higher the maximal Doppler shift $f_{D\max}$ the lower I_{E1}. The curve for $f_{D\max} = 100$ Hz starts for $I_{A1} = 0$ (no *a priori* knowledge) at a higher *a posteriori* output I_{E1} than the other two curves. But for $I_{A1} = 1$ (perfect *a priori* knowledge), all curves have nearly the same *a posteriori* output I_{E1}.

Now, we are interested in the impact of the pilot CE stage on the performance of the receiver. Therefore, we consider the trajectory of the iterative decoding loop in the EXIT chart. Generally, the trajectory shows the exchange of information between the detection stage and the decoder [3]–[7].

In Fig. 8, the EXIT chart is depicted for $f_{D\max} = 100$ Hz. The trajectory is a simulation result of the iterative scheme, whereas, the transfer characteristics are computed individually for the detection stage and the decoder, applying Gaussian distributed random variables as *a priori* inputs. The input L^{c}_{μ} to the decoder forms the mutual information I_{A2}. The *a posteriori* output $L^{c}_{d,\mu} - L^{c}_{\mu}$ of the decoder composes the mutual information I_{E2}. The achieved trajectory matches fairly well with the transfer characteristics. After one iteration the trajectory gets stuck, owing to the intersection of both characteristics at $I_{E2} \approx 1$.

In Fig. 8, the characteristic curve for a receiver with perfect channel state information (csi) is also shown. As can be seen, for perfect *a priori* knowledge $I_{A1} = 1$ the detection stage comes very close to the case of perfect csi. Therefore, the degradation in system performance due to the CE is very low.

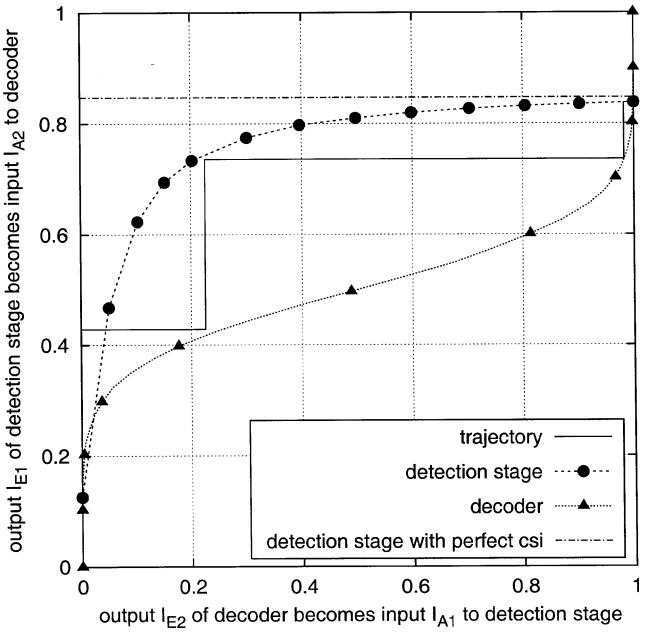

Fig. 9. EXIT chart, detection stage and decoder with simulated trajectory of the iterative decoding loop for $f_{D\max} = 300$ Hz at $E_b/N_0 = 10$ dB.

Fig. 9 shows the EXIT chart for $f_{D\max} = 300$ Hz. In comparison to Fig. 8, we need two iterations before the trajectory gets stuck, owing to the intersection of both characteristics at $I_{E2} \approx 1$. The reason is that now the two-dimensional sampling theorem is violated ($f_{D\max} > 160$ Hz). Therefore, the result of the pilot CE stage is not as good as for the case $f_{D\max} = 100$ Hz. As a consequence, the trajectory starts at a lower position (left-hand side of the chart) in comparison to Fig. 8, but although the two-dimensional sampling theorem is violated, the

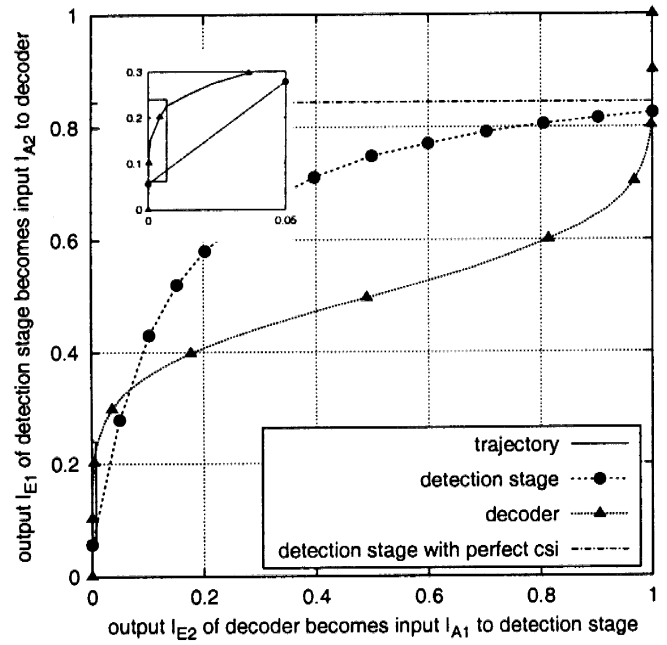

Fig. 10. EXIT chart, detection stage and decoder with simulated trajectory of the iterative decoding loop for $f_{D\max} = 600$ Hz at $E_b/N_0 = 10$ dB.

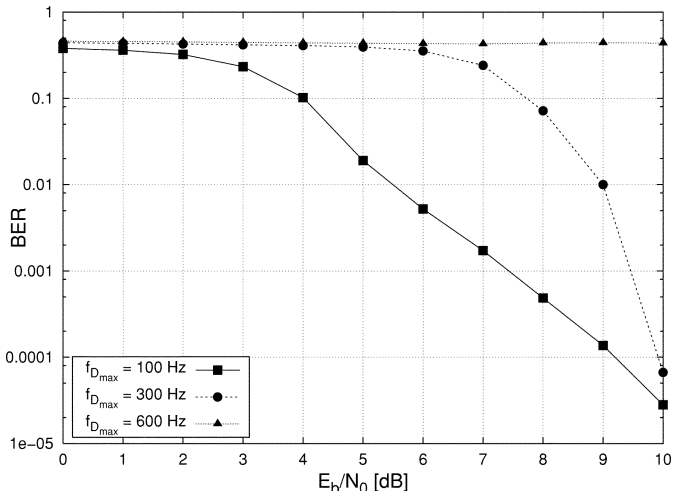

Fig. 11. BER for CE with iterative filtering and decoding after two iterations for mobile channels with various maximal Doppler shifts $f_{D\max}$.

result after two iterations still comes very close to the detection stage with perfect csi.

The trajectory for $f_{D\max} = 600$ Hz is depicted in Fig. 10. In this case, the two-dimensional sampling theorem is even more violated. As a result, the output signal of the pilot CE stage is heavily distorted. Therefore, the trajectory starts at the low position $I_{E2} = 0, I_{E1} \approx 0.25$ (see detail in Fig. 10). In the first iteration step, the trajectory drops vertically. Finally, the trajectory gets stuck on the left-hand side of the chart, owing to the intersection of both characteristics at point $I_{E2} \approx 0, I_{E1} \approx 0.05$. Thus, the performance of the receiver is very poor for $f_{D\max} = 600$ Hz.

In Fig. 11, the BER is shown after two iterations for channels with different Doppler shifts $f_{D\max}$. As expected from Fig. 10, the result of the channel estimator with iterative filtering and decoding is worse for $f_{D\max} = 600$ Hz due to the strong violation of the two-dimensional sampling theorem. So, there is no improvement of the BER by the iterative loop. Therefore, the channel estimator with iterative filtering and decoding depends on the pilot symbol spacing, i.e., on the two-dimensional sampling theorem.

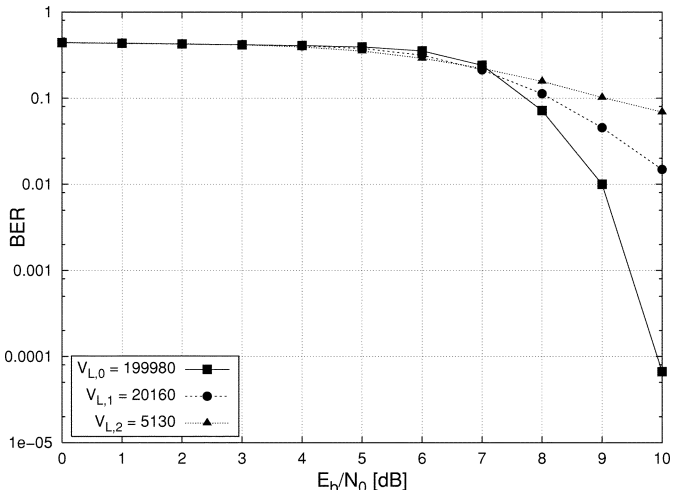

Fig. 12. BER for CE with iterative filtering and decoding after two iterations for different interleaver sizes $V_{L,i}$ at $f_{D\max} = 300$ Hz.

Fig. 12 shows the BER for different interleaver sizes $V_{L,i}$ at $f_{D\max} = 300$ Hz. To vary the interleaver size, we change the number of subcarriers K and the number of OFDM symbols L for the blockwise transmission. All the other parameters are kept. For the interleaver size $V_{L,0} = 199\,980$, we use $K_0 = 1001$ and $L_0 = 101$ as in the simulations above. The interleaver size $V_{L,1} = 20\,160$ results for $K_1 = 101$ and $L_1 = 101$. For the interleaver size $V_{L,2} = 5130$, we use $K_2 = 51$ and $L_2 = 51$.

As can be seen, an increasing interleaver size lowers the BER for $E_b/N_0 > 7$ dB.

B. Iterative APP CE

For the iterative APP CE, we consider simple prediction with $m_t = 3$ and $m_f = 2$ in (47) and (51). In Fig. 13, the mutual information transfer characteristics of the APP CE stage are depicted similar to Fig. 7. The *a priori* input $L^{\tilde{c}}_{a,\mu}$ to the APP CE stage in Fig. 5 is on the abscissa (mutual information $0 \leq I_{A1} \leq 1$ in bit per binary symbol). The *a posteriori* output $L^{\tilde{c}}_{\mu} - L^{\tilde{c}}_{a,\mu}$ is on the ordinate (mutual information $0 \leq I_{E1} \leq 1$). The mutual information transfer characteristics describe the input–output relations of the APP CE stage.

As can be seen, all curves end at a high *a posteriori* output I_{E1} for perfect *a priori* knowledge $I_{A1} = 1$. The *a posteriori* output I_{E1} is higher, the lower the maximal Doppler shift is for perfect *a priori* knowledge $I_{A1} = 1$. This aspect holds also for the beginning of the curves at $I_{A1} = 0$ (no *a priori* knowledge is available).

In Fig. 14, the EXIT chart is depicted for $f_{D\max} = 100$ Hz.

The trajectory of the iterative decoding loop shows the exchange of information between the APP CE stage and the decoder. The input L^{c}_{μ} to the decoder forms the mutual information I_{A2}. The *a posteriori* output $L^{c}_{d,\mu} - L^{c}_{\mu}$ of the decoder composes the mutual information I_{E2}. The achieved trajectory matches

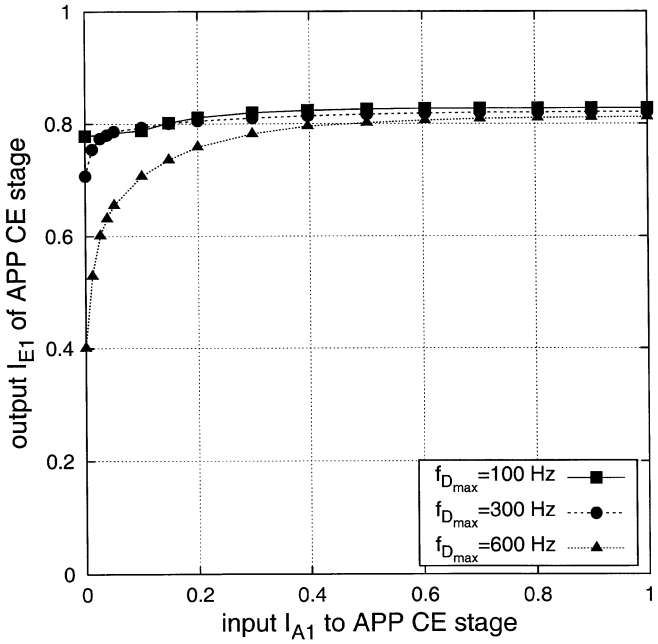

Fig. 13. Mutual information transfer characteristics of the APP CE stage for different maximal Doppler shifts $f_{D_{\max}}$ at $E_b/N_0 = 10$ dB.

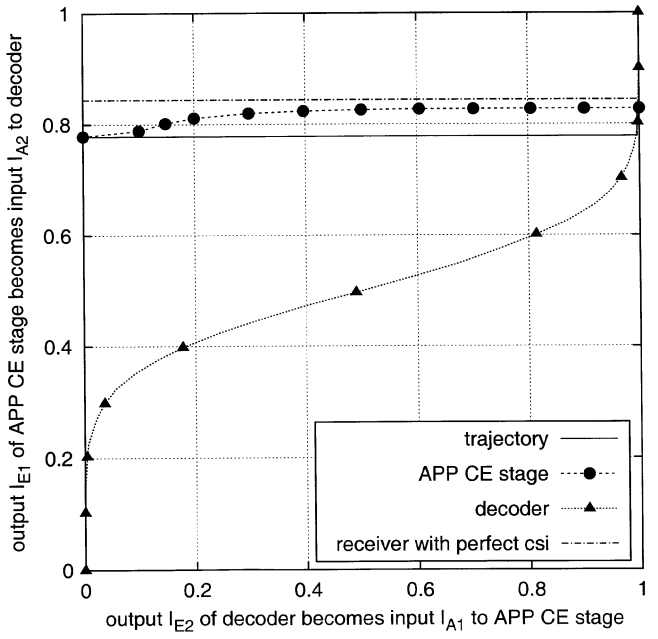

Fig. 14. EXIT chart, APP CE stage, and decoder with simulated trajectory of the iterative decoding loop for $f_{D_{\max}} = 100$ Hz at $E_b/N_0 = 10$ dB.

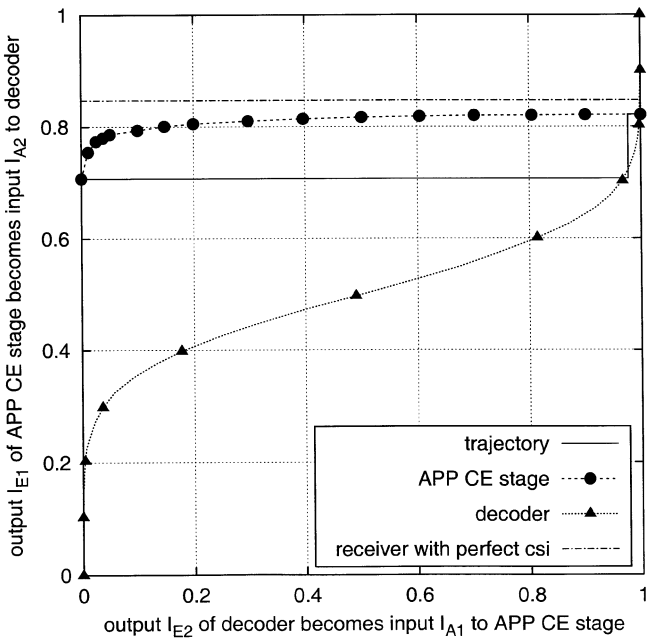

Fig. 15. EXIT chart, APP CE stage, and decoder with simulated trajectory of the iterative decoding loop for $f_{D_{\max}} = 300$ Hz at $E_b/N_0 = 10$ dB.

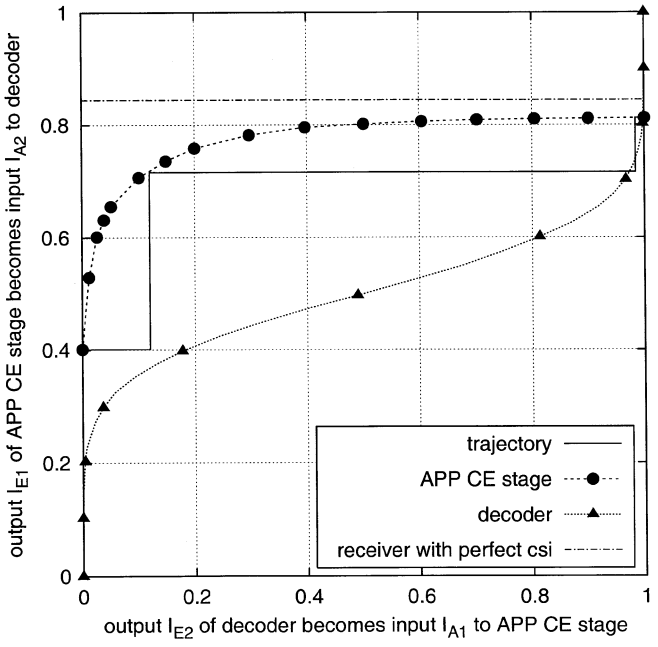

Fig. 16. EXIT chart, APP CE stage, and decoder with simulated trajectory of the iterative decoding loop for $f_{D_{\max}} = 600$ Hz at $E_b/N_0 = 10$ dB.

with the transfer characteristics fairly well. After one iteration, the trajectory gets stuck, owing to the intersection of both characteristics at $I_{E2} \approx 1, I_{E1} \approx 0.82$. In addition, the characteristic curve for a receiver with perfect csi is also shown. As can be seen, for perfect *a priori* knowledge $I_{A1} = 1$, the APP CE stage comes very close to the curve of perfect csi. Therefore, the degradation in system performance due to the CE is very low.

Fig. 15 shows the EXIT chart for $f_{D_{\max}} = 300$ Hz.

The trajectory gets stuck after about one iteration, owing to the intersection of both characteristics.

The trajectory for $f_{D_{\max}} = 600$ Hz is depicted in Fig. 16.

Also in this case, the result after about two iterations comes very close to the receiver with perfect csi.

In Fig. 17, the BER is depicted after two iterations for different maximal Doppler shifts $f_{D_{\max}}$. As can be seen, we obtain a good performance for all maximal Doppler shifts, even for $f_{D_{\max}} = 600$ Hz, although the sampling theorem is violated. This is because the iterative APP channel estimator operates on the coordinates k and l, which are upsampled by the factors D_f and D_t with respect to the pilot coordinates. Therefore, the two-dimensional sampling theorem on pilot grid basis is not decisive any more.

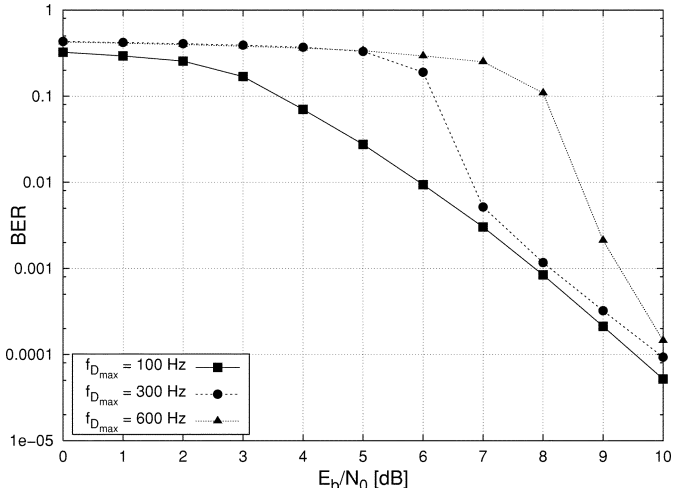

Fig. 17. BER for APP CE after two iterations for mobile channels with various maximal Doppler shifts $f_{D\max}$.

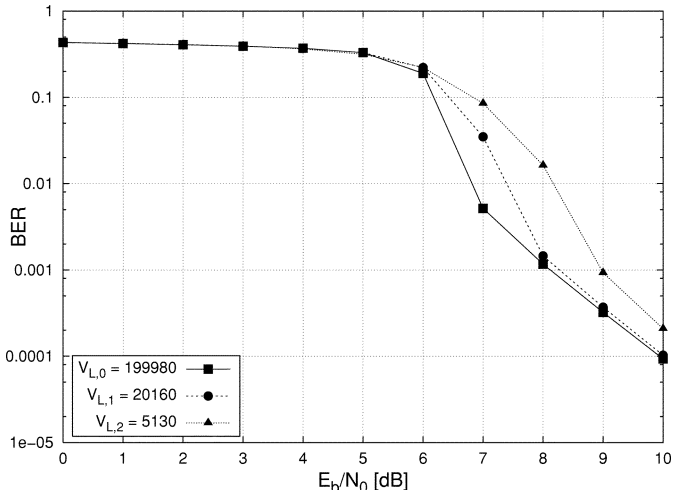

Fig. 18. BER for APP CE after two iterations for different interleaver sizes $V_{L,i}$ at $f_{D\max} = 300$ Hz.

Fig. 18 shows the simulation results after two iterations for different interleaver sizes $V_{L,i}$ at $f_{D\max} = 300$ Hz similar to Fig. 12.

As can be seen, the impact of the interleaver size on the BER is lower than for the receiver with iterative filtering and decoding (see Fig. 12). Therefore, the performance of the receiver with APP CE is superior to the receiver with iterative filtering and decoding for small interleaver sizes.

V. Conclusion

We have investigated in quite some detail two different methods for iterative estimation of the two-dimensional time-varying frequency response $H(f,t)$ of a mobile channel. The wireless transmission scheme operates with OFDM and APP soft-in/soft-out detection using likelihood values (L-values). The transmitter is equipped with a recursive convolutional encoder using a systematic code with code rate $R_c = 1/2$. To support coherent detection, pilot symbols, which form a periodic grid in the frequency-time plane, are inserted into the transmission signal. The pilot grid on the frequency axis is given by the carrier spacing Δf and on the time axis by the symbol spacing T_s. For the mobile channel, a WSSUS model is used with $H(f,t)$ in (2).

The first channel estimator with iterative filtering and decoding (Fig. 3) is an extension to the well-known CE applying Wiener Filtering [1]. The L-values on the coded bits at the output of the APP decoder are fed back to iteratively compute an improved estimate of the channel frequency response. As a result, this estimator shows good performance also for moderate maximal Doppler shifts exceeding the limit given by the sampling theorem. However, it fails finally for mobile channels with very large Doppler shift, e.g., $f_{D\max} = 600$ Hz, due to the violation of the sampling theorem.

The second method in Fig. 5 applies two APP estimators, one for the time and the other one for the frequency direction. These two estimators are embedded in an iterative loop similar to the turbo decoding principle. It is shown that this scheme performs almost like the channel estimator with iterative filtering and decoding in Fig. 3 for low to moderate maximal Doppler shifts up to about $f_{D\max} = 300$ Hz. However, for channels with very large Doppler shift, e.g., $f_{D\max} = 600$ Hz, this method outperforms the other estimator by far. This is because the iterative APP channel estimator operates on the discrete frequency k and discrete time l, which are upsampled coordinates with respect to the pilot positions. Therefore, the two-dimensional sampling theorem on pilot grid basis is not decisive any more. An in-depth investigation of the algorithm complexity was not subject of this letter. However, it can be said that the iterative APP channel estimator requires much more processing power than the algorithm with iterative filtering and decoding.

References

[1] P. Hoeher, S. Kaiser, and P. Robertson, "Two-dimensional pilot-symbol-aided channel estimation by Wiener filtering," in *Proc. ICASSP*, Munich, Germany, Apr. 1997, pp. 1845–1848.

[2] H.-J. Su and E. Geraniotis, "Improved performance of a PSAM system with iterative filtering and decoding," in *Proc. 36th Annu. Allerton Conf. Communication, Control, and Computing*, Sept. 1998, pp. 156–166.

[3] F. Sanzi and S. ten Brink, "Iterative channel estimation and decoding with product codes in multicarrier systems," in *Proc. IEEE Vehicular Technology Conf.*, Boston, MA, Sept. 2000, pp. 1338–1344.

[4] S. ten Brink, F. Sanzi, and J. Speidel, "Two-dimensional iterative APP channel estimation and decoding for OFDM systems," in *Proc. IEEE Global Communications Conf.*, San Francisco, CA, Nov. 2000, pp. 741–745.

[5] S. ten Brink, "Iterative decoding trajectories of parallel concatenated codes," in *Proc. 3rd IEEE/ITG Conf. Source and Channel Coding*, Munich, Germany, Jan. 2000, pp. 75–80.

[6] ——, "Design of serially concatenated codes based on iterative decoding convergence," in *Proc. 2nd Int. Symp. Turbo Codes*, Brest, France, Sept. 2000, pp. 319–322.

[7] ——, "Convergence behavior of iteratively decoded parallel concatenated codes," *IEEE Trans. Commun.*, vol. 49, pp. 1727–1737, Oct. 2001.

[8] P. Hoeher, "A statistical discrete-time model for the WSSUS multipath channel," *IEEE Trans. Veh. Technol.*, vol. 41, pp. 461–468, Nov. 1992.

[9] M. Sandell and O. Edfors, "A Comparative Study of Pilot-Based Channel Estimator for Wireless OFDM," Div. Signal Processing, Luleå Univ. Technol., Res. Rep. TULEA 1996:19, Sept. 1996.

[10] P. Hoeher, S. Kaiser, and P. Robertson, "Pilot-symbol-aided channel estimation in time and frequency," in *Proc. Int. Workshop Multi-Carrier Spread-Spectrum*, Apr. 1997, pp. 169–178.

[11] ——, "Pilot-symbol-aided channel estimation in time and frequency," in *Proc. 6th Communication Theory Mini-Conf.*, Nov. 1997, pp. 90–96.

[12] M. H. Hayes, *Statistical Digital Signal Processing and Modeling*. New York: Wiley, 1996.

[13] J. Hagenauer, E. Offer, and L. Papke, "Iterative decoding of binary block and convolutional codes," *IEEE Trans. Inform. Theory*, vol. 42, pp. 429–445, Mar. 1996.
[14] S. ten Brink, J. Speidel, and R.-H. Yan, "Iterative demapping for QPSK modulation," *Electron. Lett.*, vol. 34, no. 15, pp. 1459–1460, 1998.
[15] P. Hoeher and J. Lodge, "Iterative decoding/demodulation of coded DPSK systems," in *Proc. IEEE Global Telecommunications. Conf.*, Sydney, Australia, Nov. 1998, pp. 598–603.
[16] L. Bahl, J. Cocke, F. Jelinek, and J. Raviv, "Optimal decoding of linear codes for minimizing symbol error rate," *IEEE Trans. Inform. Theory*, vol. IT-20, pp. 284–287, Mar. 1974.
[17] J. H. Lodge and M. L. Moher, "Maximum likelihood sequence estimation of CPM signals transmitted over Rayleigh flat-fading channels," *IEEE Trans. Commun.*, vol. 38, pp. 787–794, June 1990.
[18] F. Sanzi and J. Speidel, "An adaptive two-dimensional channel estimator for wireless OFDM with application to mobile DVB-T," *IEEE Trans. Broadcast.*, vol. 46, pp. 128–133, June 2000.